Mesenchymal Stem Cells Suppress Kidney Injury molecule-1 Associated with Inhibition of Renal PKC/ NF-Kβ / STAT3 Fibrotic Signaling Pathway in Rats with Diabetic Nephropathy

Keywords
Mesenchymal stem cells, Type 2 Diabetes, Diabetic Nephropathy, PKC/NF-Kβ/STAT-3

Abstract

Introduction
Background: Diabetes stands as the predominant etiology behind end-stage kidney disease, commonly referred to as renal failure. The intricate interplay among oxidative stress, inflammation, and renal fibrotic changes in diabetes-induced nephropathy, particularly in instances involving and not involving the administration of mesenchymal stem cells (MSCs), remains a subject less explored in existing research.

Material and methods
Methods: Twenty-four male Wistar rats (180 and 200 grams) were randomly assigned to one of three groups (n = 8). The control group received standard laboratory chow, and the groups with T2DM received a single dose of streptozotocin, 45 mg/kg, after three weeks of pretreatment with a high-fat diet (HFD). Rats with T2DM were split into the T2DM model group and Bone marrow (BM) mesenchymal stem cells (MSCs) treated group (T2DM+MSCs) eight weeks after DM was confirmed. BM-MSCs were injected systemically at 2 × 106 cells/rat doses.

Results
Results: Diabetes significantly altered oxidative stress (MDA, SOD), inflammation (TNFα, IL-6), and kidney injury (KIM-1, NAGAL) biomarkers, a modulation that was mitigated by MSCs ($p < 0.0001$). Furthermore, diabetes-induced kidney fibrosis showed a noteworthy reduction in the presence of MSCs. A notable correlation emerged between body weight, systolic blood pressure (SBP), oxidative stress, inflammation, fibrosis, the PKC/NF-KB/STAT-3 axis, and hyperglycemia.

Conclusions
Conclusions: Our results suggest that diabetes was associated with elevated oxidative stress, inflammation, biomarkers of kidney injury, upregulation of the renal PKC/NF-KB/STAT-3 pathway, and hypertension, all countered by MSCs intervention.

Mesenchymal Stem Cells Suppress Kidney Injury molecule-1 Associated with Inhibition of Renal PKC/ NF-Kβ / STAT3 Fibrotic Signaling Pathway in Rats with Diabetic Nephropathy

Running title: **Molecular Mechanisms of Stem Cells in Diabetic Nephropathy**

Abstract

Background: Diabetes stands as the predominant etiology behind end-stage kidney disease, commonly referred to as renal failure. The intricate interplay among oxidative stress, inflammation, and renal fibrotic changes in diabetes-induced nephropathy, particularly in instances involving and not involving the administration of mesenchymal stem cells (MSCs), remains a subject less explored in existing research**. Methods:** Twenty-four male Wistar rats (180 and 200 grams) were randomly assigned to one of three groups (n = 8). The control group received standard laboratory chow, and the groups with T2DM received a single dose of streptozotocin, 45 mg/kg, after three weeks of pretreatment with a high-fat diet (HFD). Rats with T2DM were split into the T2DM model group and Bone marrow (BM) mesenchymal stem cells (MSCs) treated group (T2DM+MSCs) eight weeks after DM was confirmed. BM-MSCs were injected systemically at 2 × 106 cells/rat doses. **Results:** Diabetes significantly altered oxidative stress (MDA, SOD), inflammation (TNFα, IL-6), and kidney injury (KIM-1, NAGAL) biomarkers, a modulation that was mitigated by MSCs ($p < 0.0001$). Furthermore, diabetes-induced kidney fibrosis showed a noteworthy reduction in the presence of MSCs. A notable correlation emerged between body weight, systolic blood pressure (SBP), oxidative stress, inflammation, fibrosis, the PKC/NF-KB/STAT-3 axis, and hyperglycemia.

Conclusions: Our results suggest that diabetes was associated with elevated oxidative stress, inflammation, biomarkers of kidney injury, upregulation of the renal PKC/NF-KB/STAT-3 pathway, and hypertension, all countered by MSCs intervention.

Key Words: PKC/NF-Kβ/STAT-3, Type 2 Diabetes, Diabetic Nephropathy, Mesenchymal stem cells

1. Introduction

Diabetic kidney disease (DKD) is a significant healthcare concern in older patients with T2DM. DKD diagnosis depends on two criteria: low estimated glomerular filtration rate (eGFR<60 mL/min/1.73 m2) and albuminuria or proteinuria among patients with T2DM [1]. Diabetic nephropathy is the most common microvascular complication, which is expected to affect approximately 40–60% of diabetic individuals [2]. Diabetic kidney disease is currently the major cause of kidney failure and the single leading cause of diabetic mortality [3]. The build-up of extracellular matrix (ECM) in the glomerular mesangium and interstitium and increased glomerular membrane thickness are characteristics of irreversible diabetic kidney disease (DKD) [4, 5]. DKD also includes renal parenchyma sclerosis and scar formation [6]. Hyperglycemia and complications from diabetes prompt the transformation of renal epithelial cells into mesenchymal cells, alongside the activation of fibroblasts and pericytes [4], ultimately developing myofibroblasts. Massive amounts of collagen are secreted by the newly produced myofibroblasts, mediating glomerular sclerosis and other fibrosis, including renal vessels [7]. Furthermore, the pathway activation of the diacylglycerol (DAG)-protein kinase C (PKC) has been associated with chronic hyperglycemia and results in an increase in reactive oxygen species generation [8]. Additionally, hyperglycemia can trigger PKC activation, subsequently upregulating the production and expression of transforming growth factor-β1 (TGF-β1) [9].

PKC is widely recognized as a crucial proapoptotic protein in DNA damage-induced apoptosis [10]. Newly identified PKC isoenzymes could be linked to diverse inflammatory reactions and tissue damage. Studies propose that PKC plays a role in regulating collagen gene expression, with increased PKC expression implicated in the development of fibrotic conditions and its activation contributing to the advancement of inflammatory fibrosis [11]. PKC is recognized as a

pivotal contributor to the progression of diabetic nephropathy by activating nuclear factor kappa B (NF-κB) and TGF-β1. The activation of NF-κB/TGF-β1 may explain the abnormal ECM accumulation and the development of renal hypertrophy [12].

Moreover, inhibiting PKC in pericytes in vitro led to reduced NF-κB activation and diminished production of reactive oxygen species (ROS) [13, 14]. NF-κB is activated in diabetic nephropathy and is a critical transcription regulator for inflammatory processes within the kidneys of individuals with diabetes [15]. The activity of NF-κB is correlated with the JAK/STAT pathway and impacted by elevated ROS and hyperglycemia [16, 17].

In diabetes induced by streptozotocin (STZ), inhibition of signal transducer and activators of transcription (STAT3) reduced proteinuria, glomerular cell proliferation, and fibrotic activity [18]. Furthermore, the pathogenesis of diabetic nephropathy and chronic kidney disease (CKD) are linked to the activation of STAT3 in renal tubules. In diabetic renal tissues, STAT3 is also associated with collagen accumulation in the proximal tubular tissues and around the glomeruli [18]. Moreover, the dysregulated NF-kB and STAT pathways contribute to renal fibrosis and the development of diabetes [19].

In addition to conventional drugs such as sodium-glucose cotransporter 2 inhibitors [20], exercise, acupoint and yoga [21], research on the potential therapeutic application of stem cells in diabetic renal disorders is intriguing [22]. Some researchers believe bone marrow-mesenchymal cells (BM-MS) may protect tissues from inflammation. The beneficial effects of MSCs are attributed to their release of anti-inflammatory factors and antioxidant mediators via paracrine signaling [23].

The current study was designed to explore the potential therapeutic effect of stem cells in ameliorating diabetic nephropathy through the downregulation of inflammation, oxidative stress, and the PKC/ NF-kβ/ STAT3 fibrotic signaling pathway.

2. Materials and Methods

2.1. Animals

The research ethics committee at Princess Nourah Bint Abdulrahman University approved the research protocol number (HAP-01-R-059) on May 12, 2022. The approval was granted based on the guidelines outlined in the Guide for the Care and Use of Laboratory Animals published by the US National Institutes of Health (NIH publication No. 85-23, revised 1996). The study was conducted on male Wistar rats (8-9 weeks old) weighing 180-200 g. Throughout the acclimation period, the rats were housed in a clean environment with a 12-hour light/dark cycle, provided with standard pellets for food, and given unrestricted access to water.

2.2. Experimental Design

Twenty-four rats were utilized in the study and allocated randomly into three groups (8 rats per group) following a one-week adaptation phase. The control group (Control) consisted of non-diabetic rats fed a standard laboratory diet without treatment for 13 weeks. The T2DM was given a high-fat diet for 3 weeks and a single injection of streptozotocin, as previously described, to induce diabetes mellitus [24]. The MSCs plus T2DM group (MSCs+T2DM) received a single injection of MSCs derived from bone marrow (BM-MSCs) following 8 weeks of the induction of diabetes. Each rat in this group was administered an intravenous injection of 2×10^6 BM-MSCs.

2.2.1. Induction of T2DM

The rats were subjected to a high-fat diet (HFD) which is composed of 60 % fat, 20% CHO and 20% proteins that comprised (Casein 200g, L-cystine 3 g, Maltodextrin 125g, Sucrose 68.8, Cellulose 50g, Soybean oil25g, Sheep tallow 245g, Mineral mixture 10g, Vitamin mixture 10g, Dicalcium phosphate 13g, Calcium carbonate 5.5g, Potassium Citrate 16.5g, Choline bitrate 2g) [25, 26] for 3 weeks before the administration of streptozotocin (STZ). STZ powder was obtained from Sigma-Aldrich (St Louis, MO, USA). At the time of injection, a sterile sodium citrate buffer with a pH of 5-6 was used as the solvent for STZ. This solution was then intraperitoneally (i.p.) injected at 45 mg/kg body weight, where we proved previously that a high-fat diet and low dose of STZ induced diabetes till the end of the experiment [27, 28]. In the control group, a similar dose of the sterile prepared buffer was injected as a vehicle [29].

2.2.2. Verification of diabetes and care of diabetic rats

Diabetes in the model group was confirmed one week after STZ injection using a Randox reagent kit for determining fasting blood glucose levels (>200 mg/dL) (Randox Laboratories Ltd., Crumlin, UK.)[27].

2.2.3. Measuring systolic arterial blood pressure

An indirect measurement approach utilized a non-invasive blood pressure monitor (LE 5001 Pressure Meter, Letica Scientific Instruments, Spain). Systolic blood pressure (SBP) was assessed in conscious, thermally acclimated (for 30 min at 28°C) rats using the tail-cuff method [30]. Arterial blood pressure evaluation was conducted on the animals upon completion of the study.

2.2.4. Samples collection and scarification

By the end of week 13, the rats were anaesthetized with sodium phenobarbital anaesthesia at 40 mg/kg body weight before sacrifice [31]. Blood samples were obtained from the rat tail vein and

transferred into 10-milliliter Eppendorf tubes. Plasma was separated from the blood samples and utilized to measure the levels of various biochemical parameters including free fatty acids (FFA), triglycerides (TG), total cholesterol (CHO), high-density lipoprotein-C (HDL-C), urea, creatinine, kidney injury molecule-1 (KIM-1), neutrophil gelatinase-associated lipocalin (NGAL), malondialdehyde ((MDA) superoxide dismutase ((SOD) high-sensitive C-reactive protein (hs-CRP), and nuclear factor kappa-β (NF-κB).

The animals were sacrificed using a high dose of sodium phenobarbital, and then both kidneys were removed. The right kidney underwent histological and immunological preparation, while the left kidney was processed for biochemical measurement of PKC/ STAT3. The detection of stem cells in kidney tissues was confirmed by examining unstained sections with a fluorescent microscope.

2.2.5. Isolation and preparation of mesenchymal stem cells (MSCs)

Male Wistar rat femurs were used to isolate MSCs. After the bone marrow cavity was flushed, the mononuclear cell layer was prepared by centrifuging the collected marrow samples. These cells were cultured on plastic dishes in Dulbecco's modified Eagle's medium, supplemented with 10% fetal calf serum (DMEM; Gibco, Grand Island, NY). Every 3 days, the culture media were refreshed until reaching 70%–80% confluence. Subsequently, trypsin was used to separate the cells, which were subcultured until the fourth passage flow cytometry was used to identify the cells based on surface markers. Before transplantation, the enriched cells underwent flow cytometry analysis to confirm their purity and positive expression of CD73 and CD90, while they were negative for CD45 and CD34 phenotypic markers. The cells were then labelled with PKH26 Red Fluorescent Cell Linker Kit (Sigma Aldrich) and injected into the rat tail vein [32].

2.3. Biochemical measurements

2.3.1. Estimation of Serum Fasting Glucose, Total cholesterol (TCH), High-density Lipoprotein (HDL-C) and Low-Density Lipoprotein (LDL-C) Levels

We utilized the Rat Glucose Assay Kit (Catalog #81693) to measure serum glucose level, which operates on a multi-step reaction principle. The resulting dye is quantified by measuring absorbance at 505nm, directly correlating to glucose concentration in the rat specimen. Enzyme-linked immunosorbent assay (ELISA) was used to measure the levels of total cholesterol (CHO), high-density lipoprotein cholesterol (HDL-C), and low-density lipoprotein cholesterol (LDL-C) in serum samples. Total cholesterol (Catalog No. ABIN772507), HDL-C, and LDL-C rat ELISA Kit (Catalog No: MBS266554) were utilized. The colour intensity was measured spectrophotometrically using a microplate reader.

2.3.2. Estimation of Serum Urea and Creatinine levels

Kidney function was evaluated by measuring serum urea and creatinine using colourimetry and reagent kits (Urea Colorimetric Assay Kit Cat. No. E-BC-K329-S Houston, Texas; and Creatinine Assay Kit (Colorimetric) (ab204537) Waltham, United States).

2.3.3. Estimation of Kidney Injury Molecule-1 (KIM-1) and Neutrophil gelatinase-associated lipocalin (NGAL)

Rat Kim-1 ELISA Kit (MyBiosource, Cat. # MBS355395) and Rat NGAL ELISA Kit (MyBiosource, Cat. # MBS260195) were used to determine serum KIM-1 and NGAL. All procedures were carried out following the manufacturer's instructions.

2.3.4. Estimation of Biomarkers the Oxidative Stress, Inflammatory Biomarkers and NF-KB

All the animals' serum samples were collected, and oxidative stress and inflammatory indicators were measured. The TBARS Assay Kit (Cayman Chemical Company, Ann Arbor, MI, USA;

item 10009055) was used to determine malondialdehyde (MDA). The Superoxide Dismutase (SOD) kit (Item No. 706002, Cayman Chemical Company, Ann Arbor, MI, USA) was utilized for the measurement as directed by the manufacturer. Using an ELISA kit from BIOTANG INC (Cat. No. R6365, MA, USA), TNF-α was quantified. The IL-6 ELISA kit (Cat No. ELR-IL6-001), acquired from RayBio, GA, USA., was used to measure IL-6. Rat Nuclear Factor Kappa B (NFkB) ELISA Kit (Cat. # MBS453975, MyBiosource) was used to measure NF-κB.

2.3.5. Estimation of PKC/STAT3 using Reverse transcription and real-time quantitative Polymerase chain reaction (PCR)

The renal tissues underwent homogenization following a specified protocol to extract total RNA. Subsequently, cDNA synthesis was performed using the reverse transcription kit from Takara Biomedical Technology, Dalian, Liaoning, China. The Agilent-Stratagene Mx3000P Q-PCR System (Agilent Technologies Inc, Santa Clara County, CA, USA) was employed for PCR amplification. The resulting data were normalized to the reference β-actin gene. Primer sequences utilized were as follows: PKC-α forward, 5'-CAAGCAGTGCGTGATCAATGT-3'; PKC-α reverse, 5'-GGTGACGTGCAGCTTTTCATC-3'; STAT3 forward, 5'-CAGCAATACCATTGACCTGCC-3'; STAT3 reverse, 5'-TTTGGCTGCTTAAGGGGTGG-3'; β-actin forward: 5'-TCGTGCGTGACATTAAAGAG-3'; and reverse: 5'-ATTGCCGATAGTGATGACCT-3'.

2.3.6. Histological and immunological Assessment of Renal tissues

Collected specimens of renal tissues were fixed in 10% formal saline for a day before being dehydrated with increasing alcohol grades. As previously described, the tissues were cleared and embedded in paraffin using standard procedures [33]. Paraffin blocks were sectioned into 4 μm thick slices, and the deparaffinized sections were stained with hematoxylin and eosin (H&E).

We employed Masson staining to quantify renal collagen build-up. The slides were dipped in 0.01 M hydrochloric acid following overnight incubation with 0.1 per cent Masson (Sigma-Aldrich, Gillingham, Dorset, UK). Sections were subjected to an overnight incubation at 4 °C with anti-α SMA (Cat # PA5-85070, Thermofisher, USA) antibody for immunohistochemistry, then a 30-minute room temperature incubation with the secondary antibody. The sections were counterstained with Meyer's hematoxylin.

The quantification of collagen deposition in Masson-stained sections and the determination of the percentage of α-SMA immunostaining were performed. This analysis used the "Leica Qwin 500 C" image analyzer (Cambridge, UK) in eight non-overlapping fields for each section or group [34]. To analyze and compare the means and standard deviations of the quantitative data we used (ANOVA) and Post Hoc Analysis (Tukey Test) to analyze and compare the means and standard deviations of the quantitative data. A p-value lower than 0.05 is deemed statistically significant. The computations were performed using GraphPad Prism (version 6).

2.3.7. Statistical method

The data were expressed as mean ± standard deviation (SD) [34]. Data were processed, and then GraphPad Prism (version 6) was used for analysis. The Shapiro-Wilk test and normality plots were used to confirm that the data were normal. For variables that follow a normal distribution, the unpaired Student t-test was utilized to evaluate differences between the two groups; for variables that are not normally distributed, the Mann-Whitney test was employed. For regularly distributed variables, one-way ANOVA was employed, followed by Tukey's post hoc test; for non-normally distributed variables, non-parametric Kruskal-Wallis was utilized. The statistical analysis of Pearson correlation was employed to examine the relevance of the correlation between two distinct parameters. If $p \leq 0.05$, statistical significance was taken into account.

3. Results

3.1. Mesenchymal Stem Cells Improved Fasting Blood Glucose and Lipid Profile Associated with Increase Body Weight and Decrease SBP in Diabetic Rats

Results presented in Table 1 show that administering MSCs to T2DM rats improved their lipid profile and fasting blood glucose levels. In particular, the T2DM group had significantly higher fasting blood glucose and total cholesterol (TCH) levels than the control group ($P<0.0001$). Furthermore, there was a significant difference in HDL-C levels between the T2DM group and the control group and an increase in LDL-C levels between the diabetic group and the control group. Compared to the T2DM group, the administration of MSCs improved TCH HDL-C, LDL-C, and fasting blood glucose levels, but these changes did not entirely return to control levels ($P<0.0001$). In addition, the T2DM group showed a substantial increase in systolic blood pressure (SBP) and a significant decrease in body weight compared to the control group. ($P< 0.0001$). However, MSCs administration effectively increased body weight and decreased SBP compared to the T2DM group ($P<0.0001$).

3.2. Mesenchymal Stem Cells Attenuate Dysregulated Kidney Injury Biomarkers

The levels of urea (87.44±19.76mg/dL), creatinine (1.34±0.19mg/dL), KIM-1 (210.6±10.07pg/mL), NAGAL (312.8±13.25pg/mL) were significantly increased in T2DM compared to the corresponding values in the control groups (urea: 35.74± 5.527 mg/dL), (creatinine 0.2425± 0.1317, mg/dL), (KIM-1:100.1± 5.29 pg/mL), (NAGAL:122.8±3.01 pg/mL). Administration of MSCs was able to attenuate kidney injury that was observed by a significant decrease in the levels of urea (54.89± 8.81 mg/dL), creatinine (0.495±0.06 mg/dL), KIM-1

(127.9±13.0 pg/mL), and NAGAL (154.6 ± 10.40 pg/mL) compared to the corresponding values in the diabetic group **(Figure 2**).

3.3. MSCs Ameliorate Oxidative Stress and Inflammatory Biomarkers in Diabetic Rats

In the T2DM group, levels of MDA were significantly higher (136.7 ± 11.83mmol/mL) than in the control group (31.53 ± 9.35mmol/mL), while SOD. levels were significantly lower (41.45 ± 5.129U/mL) compared to the control group (95.15 ± 6.54U/mL). However, after the administration of MSCs, there was a noticeable decrease in MDA levels (65.29 ± 12.05mmol/mL) and an increase in SOD levels (71.15 ± 5.43U/mL) compared to the values in the T2DM group, as shown in (**Figures 3A-B)**. Moreover, (**Figures 3C-D)** revealed a significant increase in serum TNF (87.38 ± 11.50pg/mL) and IL-6 (113.5 ± 10.53pg/mL) in the T2DM group compared to the control group (TNF: 21.03 ± 3.28pg/mL and IL-6: 38.38 ± 5.05pg/mL, respectively). However, the administration of MSCs showed a significant decrease in TNFα (38.35 ± 6.25pg/mL) and IL-6 (64.80 ± 6.86pg/mL) levels compared to the T2DM group.

3.4. MSCs Attenuate the Dysregulated PKC/NF-KB/ STAT3 Pathway in Diabetic Rats

The results showed a significant increase in PKC (5.79 ± 1.40), NF-Kβ (269.10 ±16.18), and STAT3 (6.23± 0.55) compared to the control group (PKC:1.03± 0.02) NF-Kβ (114.9 ± 2.41) and STAT3 (1.022±0.012) respectively. MSCs administration significantly decreased the levels of PKC (3.06± 0.39, NF- Kβ (138.9 ± 11.3) and STAT2 (2.62 ±0.39) compared to the diabetic groups (Figure 4).

3.5. MSCs Protected Against Diabetes-induced Kidney Injury and Fibrosis

Diabetic nephropathy is marked by increased glomerular basement membrane thickness and mesangial matrix expansion, which eventually results in end-stage renal disease and renal

fibrosis [35]. Therefore, we assessed all rat groups' kidney injury and fibrosis levels (Figures 5,6 and 7). After staining with H&E (Figures 5A–F), Masson (Figures 6 A–D), and α-SMA (Figures 7A-D), kidney sections were examined by light microscopy.

Compared to standard kidney architecture (Figures 5 A, B), diabetes caused distorted renal corpuscles, dilated convoluted tubules, and dilated blood vessels. The tubular epithelial cells show small, darkly stained nuclei and vacuolated cytoplasm (Figures 5C, D). Masson-stained regions (Figure 6B) revealed coarse collagen build-up in the renal interstitium among the tubules and around blood vessels. Additionally, α-SMA immunostained sections in the diabetic group showed strong, widespread positive α-SMA immunostaining cells in the wall of the blood vessels and the renal interstitium (Fig 6 B).

MSCs treatment initially mitigated diabetic nephropathy (Figures 5 E, F). This is evidenced by the quantification of collagen deposition in the renal interstitium of sections stained with Masson (Figure 6C), which demonstrated an effective ($p < 0.0001$) inhibition of collagen build-up by MSCs to levels comparable to the control group. Also, MSCs administration showed minimal positive α-SMA immunostaining in the wall of the blood vessels and in the renal interstitium, which denotes the reduction of interstitial α-SMA positive cells that are engaged in the development of interstitial fibrosis (Figures 7A-D) [36]. Morphometry showed that MSCs decreased collagen deposition by reducing the Masson trichome standing and the α -SMA immunostaining area %.

3.6. Correlation results

Results showed a positive correlation between increased glycemia versus creatinine, urea, MDA, and IL-6 (A, B, C, and D) and a positive correlation between NAGAL versus urea and creatinine (Figures 8 E and F) ($P< 0.0001$, $n=24$ for all) (Figure 8).

4. Discussion

The immunomodulatory effects of MSCs were investigated in the current study to combat the advancement of diabetic renal injury and fibrosis in an animal model of diabetic nephropathy. Specifically, the study targets critical pathways, including PKC/NF-KB/STAT3, along with α-smooth muscle actin and the circulating kidney injury molecule-1 and NGAL, to assess their involvement in the progression of diabetic kidney damage, as shown in Figure 9. The advancement toward organ failure is characterized by fibrosis and structural deterioration in solid organs, notably in the kidney. In nearly all cases of progressive CKDs, the primary features consistently linked with functional decline in the glomerular filtration rate include the extent of glomerulosclerosis, tubulointerstitial fibrosis, vascular damage, and proteinuria [37]. Hence, in a rat model of T2DM-induced nephropathy, we assessed renal impairment, renal damage, and fibrosis mediated by the renal PKC/STAT3 axis without and with MSCs treatment in the current study. MSCs have been shown to have pleiotropic effects, which include antioxidative capabilities.

Furthermore, in this animal model, we investigated the relationship between the pathophysiology of T2DM-induced nephropathy, renal impairment, and glycemia. We triggered renal damage in rats by T2DM. Twelve weeks after the development of diabetes in rats, we observed that diabetes could trigger renal PKC/STAT3 axis-mediated renal dysfunction, kidney damage, and fibrosis. Our results suggest that MSCs can suppress the PKC/STAT3 axis. Also, the results of our study indicate a significant link between glycemia, renal dysfunction, and kidney injury biomarkers such as NAGAL, urea, and creatinine. This study highlights the crucial connection

between renal dysfunction and the onset of kidney injury in diabetes, emphasizing the renal protective effects of MSCs.

Diabetic nephropathy stands as one of the prevalent comorbidities accompanying T2DM and stands as a primary contributor to end-stage renal disease [38, 39]. The persistent hyperglycemia associated with diabetes [40] is implicated in glomerular dysfunction by activating PKC [13]. The role of PKC in eliciting structural alterations secondary to chronic hyperglycemia has been extensively investigated. In light of this research point's current understanding, we focus on elucidating how hyperglycemia influences PKC activation. Notably, PKCs can be triggered by heightened production of oxidant factors, with increased oxidative stress often linked to mitochondrial dysfunction induced by elevated glucose levels [41].

Numerous aberrant vascular and cellular processes and dysregulations, including endothelial dysfunction, increased permeability of blood vessels, aberrant cell growth, apoptosis, increased thickness of basement membrane, and extracellular matrix expansion, have been observed in diabetic nephropathy [13]. Our study aims to evaluate the levels of glycemia, dyslipidemia, inflammation, and oxidative stress biomarkers in rats with experimentally induced diabetes with or without MSC treatment. Our results demonstrate that MSC administration attenuated kidney fibrosis in diabetic rats, as evidenced by decreased collagen deposition observed in Masson trichrome staining and α-SMA immunostaining. The current results also highlighted the reno-protective effects of BM-MSCs as a significant decrease in urea, creatinine, KIM-1, and NGAL levels are observed.

The current findings underscore the renal protective effects of BM-MSCs, evident through a notable reduction in urea, creatinine, KIM-1, and NGAL levels. KIM-1, a type I transmembrane glycoprotein primarily expressed on the proximal epithelial cells of renal tubules, remains

undetectable under normal conditions [42]. However, following renal injury, serum levels exhibit a significant increase. KIM-1 serves as a marker for differentiation and proliferation [43]. Our results show a positive correlation between KIM-1 levels and glycemia.

NGAL, on the other hand, serves as a structural tubular marker and exhibits extensive elevation in serum or urine shortly after ischemia-reperfusion injury. Several preclinical and clinical cohort studies have highlighted a positive correlation between NGAL and the severity of albuminuria or renal impairment [44]. NGAL emerges as a promising marker for acute and chronic kidney diseases, with reference standards suggesting its utility in diagnosing diabetic kidney diseases [45]. Results from our study show a significant elevation in NGAL levels in the T2DM group compared to the control, alongside a positive correlation between NGAL levels and urea and creatinine, indicating the occurrence of kidney injury in diabetic rats.

Mesenchymal stem cells have showcased their therapeutic potential in various animal and clinical trials. They present diverse modalities for addressing T2DM. With their low immunogenicity, self-renewal capacity, and ability to differentiate, MSCs exhibit specific antidiabetic effects [46]. Apart from their secretion of cytokines, growth factors, and exosomes, MSCs significantly impact insulin sensitivity and β-cell dysfunction [47]. Our findings show that MSCs could reduce blood glucose levels with a single-dose infusion.

The pathogenesis of obesity-related insulin resistance, which underlies T2DM, involves chronic low-grade inflammation and immune system activation [48]. These alterations are marked by chronic overexpression of pro-inflammatory cytokines [49] like TNF-α, IL-6, and interleukin-1β, contributing to metabolic syndromes and T2DM development [47].

Additionally, prolonged hyperglycemia and insulin resistance are critical factors in diabetic vascular complications. Results from this study show that hyperglycemia triggers oxidative

stress, activating PKC and initiating a pro-inflammatory response via NF-κB activation [16]. Consecutively, increased oxidative stress initiates pro-inflammatory response via activation of NF-κβ [50]. In hyperglycemic conditions, NF-κB activity is significantly enhanced, releasing cytokines and vascular adhesion molecules [51]. Previous research indicates an enhanced renal NF-κB system in CKD, which is also engaged in the pathogenesis of DKD. Inhibition of NF-κB may attenuate kidney injury and inflammation in various experimental models [52]. Hyperglycemia-induced NF-κB-mediated kidney inflammation through activating the PI3K/AKT-ERK signaling pathway in glomerular mesangial cells has been observed. Interruption of these vicious cycles may prevent DKD development in diabetics [53].

Mesenchymal stem cells are known for their antifibrotic effects and ability to reduce scar and fibrosis, achieved through upregulation of antiproliferation-related genes rather than direct modulation of the extracellular matrix (ECM) produced by fibroblasts [54]. The pharmacologic induction of DKD with STZ combined with a high-fat diet is a standard rodent model used to study potential MSCs therapy (38). Progressive tubulointerstitial fibrosis is a recognizable feature of nearly all forms of CKD and represents the final common pathway (39). MSCs and their conditioned medium have shown promise in attenuating renal fibrosis in various models [55].

Here, we demonstrated that MSCs administration inhibits NFκB production in the diabetic group, consistent with previous research indicating that MSCs can attenuate nephropathy by inhibiting oxidative stress and alleviating inflammation via NFκB inhibition [56]. In vitro, cultivating activated human neutrophils in MSC-created media reduced IL-6 and macrophage inflammatory protein 2 release [57]. This agrees with our results, where we showed that the administration of stem cells to diabetic rats decreased TNFα and IL-6. Furthermore, we observed

that MSCs administration improved diabetic status, decreased glucose levels and dysregulated lipid profiles, and provided renal protection, evidenced by reductions in serum urea, creatinine, and renal fibrosis. Molecular detection revealed reduced renal fibrosis-related indicators and α-SMA expression in the MSCs-treated group. Moreover, MSCs transplantation in diabetic rats significantly reduced STAT3 renal expression levels, suggesting a potential STAT3-dependent mechanism for reducing renal fibrosis. This agrees with the previously reported role of STAT3 in mediating the profibrotic signaling pathway [58].

There are certain limitations to this study, even with our innovative findings. Future studies will successfully identify more pathways regulating inflammatory biomarkers in different regions of the kidneys. Examining this effect on kidney function and all other observed markers over an extended period may be more illuminating. Moreover, this study merely showed that MSCs may have a preventive impact against heart injury. This study did not assess MSCs' capacity to shield the heart, liver, lungs, or blood vessels from the adverse effects of diabetes; however, we will investigate this issue in future research.

5. Conclusions

Results from our study delineated the exacerbation of oxidative stress and inflammatory mediators concomitant with elevated kidney injury markers alongside the upregulation of renal PKC/STAT3 expression and NF-κB-mediated renal fibrosis in an experimental rat model of diabetic nephropathy. MSCs, recognized for their multifaceted therapeutic potential, exhibited profound modulatory effects transcending their established antidiabetic properties. Our results suggest that MSCs abrogate several deleterious pathways pivotal in the progression of renal

dysfunction, encouraging further research of their therapeutic utility in diabetic nephropathy management.

6. Study limitations

However, even though we came up with some novel discoveries, our study does have limitations. First, when the MSCs have been cultured, the soluble mediators produced in the supernatant, including IL-4, IL-12, and TGF-beta, should be quantified and then injected into the animals with diabetes. In the future, research should be conducted to examine this topic to determine whether or not renal injury and fibrosis may be successfully minimized and to find additional pathways that regulate inflammatory and fibrotic indicators in various kidney regions. A more valuable condition would be to investigate this effect on kidney function and all other observable markers over a longer length of time. The findings of this study just demonstrated that MSCs may have a preventative effect against kidney injury. Even though this study did not investigate whether MSCs can protect the heart, liver, lungs, or blood vessels from the negative consequences of diabetes, additional research will be required.

Furthermore, measuring other dependable oxidative stress markers, such as GSH in both the tissues and the serum, is necessary. In addition, the diabetes status of rats should be monitored at intervals other than one week. This would clearly illustrate the development of a diabetic model and eliminate the concern about euglycemia on the seventh day of STZ treatment (45 mg/kg). Along with renal damage molecules, urine albumin excretion should be examined.

Funding: This research was funded by the Deanship of Scientific Research at Princess Nourah bint Abdulrahman University through the Research Funding Program, Grant No. (FRP-1443-23).

Acknowledgements

We thank Yasmeen Haidara, American University Cairo (AUC), Egypt, for proofreading the manuscript.

Conflicts of Interest

The authors confirm that this article's content has no conflict of interest.

References

1. Kitaoka K, Yano Y, Nagasu H, Kanegae H, Chishima N, Akiyama H, et al. Kidney outcomes of SGLT2 inhibitors among older patients with diabetic kidney disease in real-world clinical practice: the Japan Chronic Kidney Disease Database Ex. BMJ Open Diabetes Res Care 2024; 12.
2. Wagnew F, Eshetie S, Kibret GD, Zegeye A, Dessie G, Mulugeta H, et al. Diabetic nephropathy and hypertension in diabetes patients of sub-Saharan countries: a systematic review and meta-analysis. BMC Res Notes 2018; 11: 565.
3. Gheith O, Farouk N, Nampoory N, Halim MA, Al-Otaibi T. Diabetic kidney disease: world wide difference of prevalence and risk factors. J Nephropharmacol 2016; 5: 49-56.
4. Lin YC, Chang YH, Yang SY, Wu KD, Chu TS. Update of pathophysiology and management of diabetic kidney disease. J Formos Med Assoc 2018; 117: 662-675.
5. Quan N, Guo J. Mechanism of tangshen formula in treating diabetic nephropathy revealed by network pharmacology approach. Arch Med Sci 2021; 17: 1436-1439.
6. Sun J, Wang Y, Cui W, Lou Y, Sun G, Zhang D, et al. Role of Epigenetic Histone Modifications in Diabetic Kidney Disease Involving Renal Fibrosis. J Diabetes Res 2017; 2017: 7242384.
7. Zhang Y, Jin D, Duan Y, Zhang Y, Duan L, Lian F, et al. Bibliometric Analysis of Renal Fibrosis in Diabetic Kidney Disease From 1985 to 2020. Front Public Health 2022; 10: 767591.
8. Noh H, King GL. The role of protein kinase C activation in diabetic nephropathy. Kidney Int Suppl 2007: S49-53.
9. Isaka Y. Targeting TGF-β Signaling in Kidney Fibrosis. Int J Mol Sci 2018; 19.

10. Pabla N, Dong G, Jiang M, Huang S, Kumar MV, Messing RO, et al. Inhibition of PKCδ reduces cisplatin-induced nephrotoxicity without blocking chemotherapeutic efficacy in mouse models of cancer. J Clin Invest 2011; 121: 2709-2722.

11. Lee SJ, Kim SJ, Lee HS, Kwon OS. PKCδ Mediates NF-κB Inflammatory Response and Downregulates SIRT1 Expression in Liver Fibrosis. Int J Mol Sci 2019; 20.

12. Ghaiad HR, Ali SO, Al-Mokaddem AK, Abdelmonem M. Regulation of PKC/TLR-4/NF-kB signaling by sulbutiamine improves diabetic nephropathy in rats. Chem Biol Interact 2023; 381: 110544.

13. Geraldes P, King GL. Activation of protein kinase C isoforms and its impact on diabetic complications. Circ Res 2010; 106: 1319-1331.

14. Ismail AMA, Abd Elfatah Abo Saif HF, El-Moatasem Mohamed AM. Effect of Jyoti-Trataka on intraocular pressure, autonomic control, and blood glucose in diabetic patients with high-tension primary open-angle glaucoma: a randomized-controlled trial. J Complement Integr Med 2022; 19: 1013-1018.

15. Song N, Thaiss F, Guo L. NFκB and Kidney Injury. Front Immunol 2019; 10: 815.

16. García-García PM, Getino-Melián MA, Domínguez-Pimentel V, Navarro-González JF. Inflammation in diabetic kidney disease. World J Diabetes 2014; 5: 431-443.

17. Ren Y, Yu M, Zheng D, He W, Jin J. Lysozyme promotes renal fibrosis through the JAK/STAT3 signal pathway in diabetic nephropathy. Arch Med Sci 2024; 20: 233-247.

18. Zheng C, Huang L, Luo W, Yu W, Hu X, Guan X, et al. Inhibition of STAT3 in tubular epithelial cells prevents kidney fibrosis and nephropathy in STZ-induced diabetic mice. Cell Death Dis 2019; 10: 848.

19. Lazaro I, Oguiza A, Recio C, Mallavia B, Madrigal-Matute J, Blanco J, et al. Targeting HSP90 Ameliorates Nephropathy and Atherosclerosis Through Suppression of NF-κB and STAT Signaling Pathways in Diabetic Mice. Diabetes 2015; 64: 3600-3613.

20. Chung JF, Yang PJ, Chang CK, Lee CY, Huang JY, Wang K, et al. The use of sodium-glucose cotransporter 2 inhibitors and the incidence of uveitis in type 2 diabetes: a population-based cohort study. Arch Med Sci 2024; 20: 402-409.

21. Ismail AMA, El-Azeim ASA. Short-Term Intraocular Pressure Response to the Combined Effect of Transcutaneous Electrical Nerve Stimulation over Acupoint (Acu-TENS) and Yoga Ocular Exercise in Type 2 Diabetic Patients with Primary Open-Angle Glaucoma: A Randomized Controlled trial. J Acupunct Meridian Stud 2021; 14: 193-199.

22. Zheng S, Zhang K, Zhang Y, He J, Ouyang Y, Lang R, et al. Human Umbilical Cord Mesenchymal Stem Cells Inhibit Pyroptosis of Renal Tubular Epithelial Cells through miR-342-3p/Caspase1 Signaling Pathway in Diabetic Nephropathy. Stem Cells Int 2023; 2023: 5584894.

23. Han Y, Yang J, Fang J, Zhou Y, Candi E, Wang J, et al. The secretion profile of mesenchymal stem cells and potential applications in treating human diseases. Signal Transduct Target Ther 2022; 7: 92.

24. Reed MJ, Meszaros K, Entes LJ, Claypool MD, Pinkett JG, Gadbois TM, et al. A new rat model of type 2 diabetes: the fat-fed, streptozotocin-treated rat. Metabolism 2000; 49: 1390-1394.

25. Preguiça I, Alves A, Nunes S, Fernandes R, Gomes P, Viana SD, et al. Diet-induced rodent models of obesity-related metabolic disorders—A guide to a translational perspective. Obesity Reviews 2020; 21: e13081.

26. Evans CC, LePard KJ, Kwak JW, Stancukas MC, Laskowski S, Dougherty J, et al. Exercise prevents weight gain and alters the gut microbiota in a mouse model of high fat diet-induced obesity. PloS one 2014; 9: e92193.

27. Dawood AF, Maarouf A, Alzamil NM, Momenah MA, Shati AA, Bayoumy NM, et al. Metformin Is Associated with the Inhibition of Renal Artery AT1R/ET-1/iNOS Axis in a Rat Model of Diabetic Nephropathy with Suppression of Inflammation and Oxidative Stress and Kidney Injury. Biomedicines 2022; 10: 1644.

28. Dawood AF, Alzamil NM, Hewett PW, Momenah MA, Dallak M, Kamar SS, et al. Metformin Protects against Diabetic Cardiomyopathy: An Association between Desmin-Sarcomere Injury and the iNOS/mTOR/TIMP-1 Fibrosis Axis. Biomedicines 2022; 10: 984.

29. TME AE, Shati AA, Alqahtani SA, Ebrahim HA, Almohaimeed HM, ShamsEldeeen AM, et al. Mesenchymal stem cells improve cardiac function in diabetic rats by reducing cardiac injury biomarkers and downregulating JAK/STAT/iNOS and iNOS/Apoptosis signaling pathways. Molecular and cellular endocrinology 2024; 591: 112280.

30. ShamsEldeen AM, Fawzy A, Ashour H, Abdel-Rahman M, Nasr HE, Mohammed LA, et al. Hibiscus attenuates renovascular hypertension-induced aortic remodeling dose dependently: the oxidative stress role and Ang II/cyclophilin A/ERK1/2 signaling. Front Physiol 2023; 14: 1116705.

31. Alamri HS, Mufti R, Sabir DK, Abuderman AA, Dawood AF, ShamsEldeen AM, et al. Forced Swimming-Induced Depressive-like Behavior and Anxiety Are Reduced by Chlorpheniramine via Suppression of Oxidative and Inflammatory Mediators and Activating the Nrf2-BDNF Signaling Pathway. Curr Issues Mol Biol 2023; 45: 6449-6465.

32. ShamsEldeen AM, El-Aal SAA, Aboulhoda BE, AbdAllah H, Gamal SM, Hassan FE, et al. Combined Systemic Intake of K-ATP Opener (Nicorandil) and Mesenchymal Stem Cells Preconditioned With Nicorandil Alleviates Pancreatic Insufficiency in a Model of Bilateral Renal Ischemia/Reperfusion Injury. Front Physiol 2022; 13: 934597.

33. Shati AA, Zaki MSA, Alqahtani YA, Haidara MA, Al-Shraim M, Dawood AF, et al. Potential Protective Effect of Vitamin C on Qunalphos-Induced Cardiac Toxicity: Histological and Tissue Biomarker Assay. Biomedicines 2021; 10: 39

34. Cooper DC, Tomfohr LM, Milic MS, Natarajan L, Bardwell WA, Ziegler MG, et al. Depressed mood and flow-mediated dilation: a systematic review and meta-analysis. Psychosom Med 2011; 73: 360-369.

35. Kriz W, Löwen J, Federico G, van den Born J, Gröne E, Gröne HJ. Accumulation of worn-out GBM material substantially contributes to mesangial matrix expansion in diabetic nephropathy. Am J Physiol Renal Physiol 2017; 312: F1101-f1111.

36. Bijkerk R, Au YW, Stam W, Duijs J, Koudijs A, Lievers E, et al. Long Non-coding RNAs Rian and Miat Mediate Myofibroblast Formation in Kidney Fibrosis. Front Pharmacol 2019; 10: 215.

37. Sharma K, Zhang G, Hansen J, Bjornstad P, Lee HJ, Menon R, et al. Endogenous adenine mediates kidney injury in diabetic models and predicts diabetic kidney disease in patients. J Clin Invest 2023; 133: e170341.

38. Warren AM, Knudsen ST, Cooper ME. Diabetic nephropathy: an insight into molecular mechanisms and emerging therapies. Expert Opin Ther Targets 2019; 23: 579-591.

39. Ekiz-Bilir B, Bilir B, Aydın M, Soysal-Atile N. Evaluation of endocan and endoglin levels in chronic kidney disease due to diabetes mellitus. Arch Med Sci 2019; 15: 86-91.

40. Ismail A, Shaaban Abd El-Azeim A. Immediate fasting blood glucose response to electroacupuncture of ST36 versus CV 12 in patients with type 2 diabetes mellitus: randomized controlled trial. Family Medicine & Primary Care Review 2021; 23: 437-441.

41. An Y, Xu BT, Wan SR, Ma XM, Long Y, Xu Y, et al. The role of oxidative stress in diabetes mellitus-induced vascular endothelial dysfunction. Cardiovasc Diabetol 2023; 22: 237.

42. Kin Tekce B, Tekce H, Aktas G, Sit M. Evaluation of the urinary kidney injury molecule-1 levels in patients with diabetic nephropathy. Clin Invest Med 2014; 37: E377-383.

43. Khan FA, Fatima SS, Khan GM, Shahid S. Evaluation of kidney injury molecule-1 as a disease progression biomarker in diabetic nephropathy. Pak J Med Sci 2019; 35: 992-996.

44. He P, Bai M, Hu JP, Dong C, Sun S, Huang C. Significance of Neutrophil Gelatinase-Associated Lipocalin as a Biomarker for the Diagnosis of Diabetic Kidney Disease: A Systematic Review and Meta-Analysis. Kidney Blood Press Res 2020; 45: 497-509.

45. Kaul A, Behera MR, Rai MK, Mishra P, Bhaduaria DS, Yadav S, et al. Neutrophil Gelatinase-associated Lipocalin: As a Predictor of Early Diabetic Nephropathy in Type 2 Diabetes Mellitus. Indian J Nephrol 2018; 28: 53-60.

46. Zhang Y, Cai W, Huang Q, Gu Y, Shi Y, Huang J, et al. Mesenchymal stem cells alleviate bacteria-induced liver injury in mice by inducing regulatory dendritic cells. Hepatology 2014; 59: 671-682.

47. Gao S, Zhang Y, Liang K, Bi R, Du Y. Mesenchymal Stem Cells (MSCs): A Novel Therapy for Type 2 Diabetes. Stem Cells Int 2022; 2022: 8637493.

48. Esser N, Legrand-Poels S, Piette J, Scheen AJ, Paquot N. Inflammation as a link between obesity, metabolic syndrome and type 2 diabetes. Diabetes Res Clin Pract 2014; 105: 141-150.

49. Tomé-Carneiro J, Larrosa M, Yáñez-Gascón MJ, Dávalos A, Gil-Zamorano J, Gonzálvez M, et al. One-year supplementation with a grape extract containing resveratrol modulates inflammatory-related microRNAs and cytokines expression in peripheral blood mononuclear cells of type 2 diabetes and hypertensive patients with coronary artery disease. Pharmacol Res 2013; 72: 69-82.

50. Lv X, Lv GH, Dai GY, Sun HM, Xu HQ. Food-advanced glycation end products aggravate the diabetic vascular complications via modulating the AGEs/RAGE pathway. Chin J Nat Med 2016; 14: 844-855.

51. Suryavanshi SV, Kulkarni YA. NF-κβ: A Potential Target in the Management of Vascular Complications of Diabetes. Front Pharmacol 2017; 8: 798.

52. Okabe C, Borges RL, de Almeida DC, Fanelli C, Barlette GP, Machado FG, et al. NF-κB activation mediates crystal translocation and interstitial inflammation in adenine overload nephropathy. Am J Physiol Renal Physiol 2013; 305: F155-163.

53. Foresto-Neto O, Albino AH, Arias SCA, Faustino VD, Zambom FFF, Cenedeze MA, et al. NF-κB System Is Chronically Activated and Promotes Glomerular Injury in Experimental Type 1 Diabetic Kidney Disease. Front Physiol 2020; 11: 84.

54. Ohnishi S, Sumiyoshi H, Kitamura S, Nagaya N. Mesenchymal stem cells attenuate cardiac fibroblast proliferation and collagen synthesis through paracrine actions. FEBS Lett 2007; 581: 3961-3966.

55. Liu B, Hu D, Zhou Y, Yu Y, Shen L, Long C, et al. Exosomes released by human umbilical cord mesenchymal stem cells protect against renal interstitial fibrosis through ROS-mediated P38MAPK/ERK signaling pathway. Am J Transl Res 2020; 12: 4998-5014.

56. Song IH, Jung KJ, Lee TJ, Kim JY, Sung EG, Bae YC, et al. Mesenchymal stem cells attenuate adriamycin-induced nephropathy by diminishing oxidative stress and inflammation via downregulation of the NF-kB. Nephrology (Carlton) 2018; 23: 483-492.

57. Sarsenova M, Kim Y, Raziyeva K, Kazybay B, Ogay V, Saparov A. Recent advances to enhance the immunomodulatory potential of mesenchymal stem cells. Front Immunol 2022; 13: 1010399.

58. Li Y, Luo C, Zeng Y, Zheng Z, Tao D, Liu Q, et al. Renal Fibrosis Is Alleviated through Targeted Inhibition of IL-11-Induced Renal Tubular Epithelial-to-Mesenchymal Transition. Am J Pathol 2023; 193: 1936-1952.

Table legend:

Table 1. MSCs improved fasting blood glucose lipid profile, body weight and SBP in T2DM animals.

Changes in fasting blood glucose, TCH, TG, cholesterol, and HDL-c in control, T2DM, T2DM+MSCs groups. Data presented as mean ± SD **a**: statistically significant compared to the corresponding value in the control group (P<0.0001), and **b**: statistically significant compared to the corresponding value in the T2DM group (P<0.0001) (n=8).

Figure legends:

Figure 1. BM-MSC identification and characteristics (**A)** The isolated and grown MSCs were identified based on their immunological features; they were positive for CD90 and CD73 but negative for CD45 and CD34. (B) BM-MSC characteristics and identification Using a fluorescence microscope to examine cardiac tissue sections, it was possible to see that BM-MSCs labelled with PKH26 fluorescent dye had homing properties (red fluorescence).

Figure 2. Changes in serum urea (A), creatinine (B), and the indicators of kidney injury KIM-1 (C) and NAGAL (D) in control, T2DM, T2DM+MSCs groups. The data are presented as mean ± SD *: statistically significant in comparison to the control group's corresponding value (P<0.0001) and statistically significant in comparison to the T2DM group's corresponding value (P<0.0001) (n=8).

Figure 3. Serum MDA (A) and SOD (B), TNF (C) and IL-6 (D) levels changed in the contro, T2DM, and T2DM+MSC groups. The data are displayed as mean ± SD *: statistically significant when compared to the comparable value in the control group (P<0.0001) and the T2DM group (P<0.0001) (n=8).

Figure 4. PKC (A), and STAT3 (C) levels were quantified by PCR and NF-KB (B) by ELISA in control, T2DM, and T2DM+MSCs groups. Results are displayed as mean ± SD *: statistically significant when compared to the equivalent value in the control group (P<0.0001) and the T2DM group (P<0.0001) (n=8).

Figure 5. Photomicrographs of H&E-stained sections of the renal cortex. (A, B) Proximal (P) and distal (D) convoluted tubules bordered with cuboidal cells displaying vesicular nuclei (v) and acidophilic cytoplasm; Malpighian renal corpuscle with glomerulus (G); and narrow Bowman's space (arrow) comprise the control group. (A, D) Diabetic group: dilated convoluted

tubules (wavy arrow), dilated blood vessels (B), and deformed renal corpuscles (arrowhead). Vacuolated cytoplasm (curved arrow) and tiny, darkly-stained nuclei (P) are visible in the tubular epithelial cells. (F, E) The group known as T2DM+MSCs consists of proximal (P) and distal (D) convoluted tubules bordered with cuboidal cells that display vesicular (v) and acidophilic cytoplasm, but some cells also have pyknotic nuclei (P). There are a few dilated convoluted tubules visible (wavy arrow). (a, d, f ×400; c, e, ×200) (50 µm and 20 µm scale bars).

Figure 6. Photomicrographs of Masson-stained sections of the renal cortex. (A) Collagen deposition (arrow) in the glomerulus' interstitium represents the control group. (B) Diabetic group: coarse collagen deposition (arrow) in the deformed glomeruli and renal interstitium between tubules and blood vessels (B). (C) T2DM+MSCs group: modest localized collagen deposition in the glomeruli and convoluted tubules. (×200) (50 µm scale bar) (D) Calculating the average area percentage of the collagen deposit.

Figure 7. Photomicrographs of α-SMA-stained sections in the renal cortex. (A) Control group blood vessel walls with modest positive α-SMA immunostaining (arrow). (B) Diabetic group: renal interstitium and blood vessel walls show coarse, widespread positive α-SMA immunostaining (arrow). Minimal positive α-SMA immunostaining (arrow) in the renal interstitium and blood vessel walls (C) T3DM+MSCs group. (×200) (50 µm scale bar). (D) Calculating the average percentage of α-SMA immunostaining area.

Figure 8. Correlation results Positive correlation between glycemia versus creatinine, urea, MDA and IL-6 (A-D). Positive correlation between NAGAL versus urea and creatinine (E-F) ($P < 0.0001$, n=24).

Figure 9. Injection of MSCs ameliorated and improved the parameters of diabetic nephropathy.

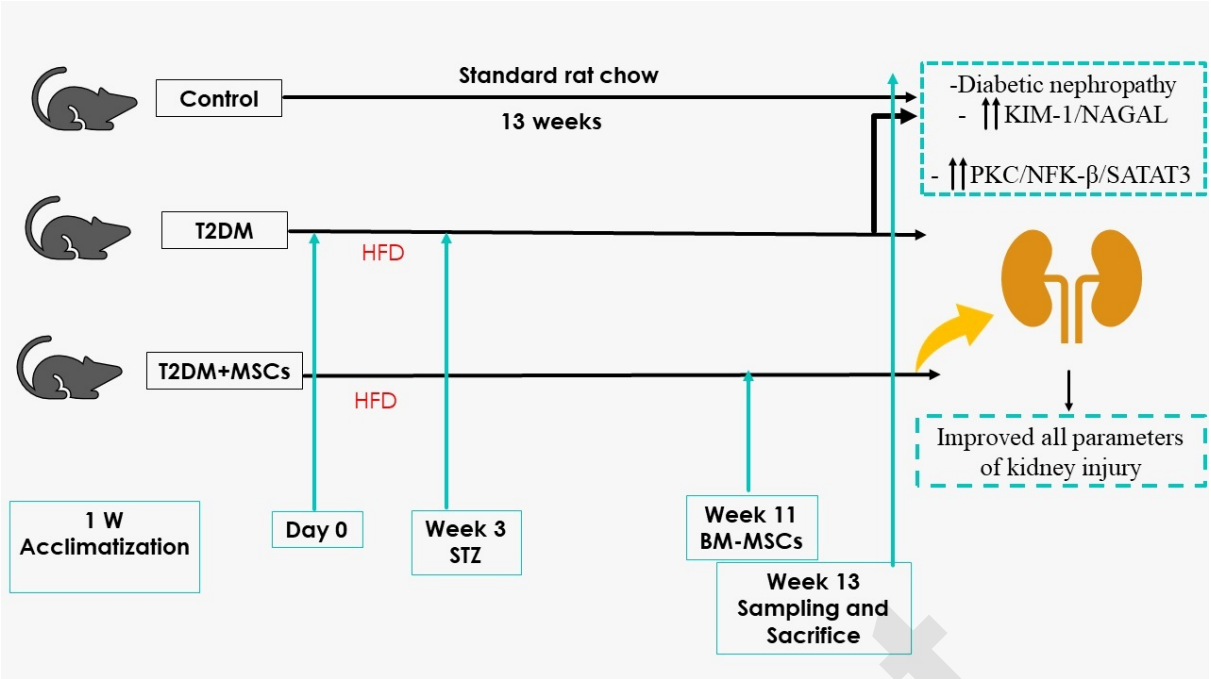
Control
Standard rat chow
13 weeks
T2DM
HFD
T2DM+MSCs
HFD
-Diabetic nephropathy
- ↑↑KIM-1/NAGAL
- ↑↑PKC/NFK-β/SATAT3
Improved all parameters of kidney injury
1 W Acclimatization
Day 0
Week 3 STZ
Week 11 BM-MSCs
Week 13 Sampling and Sacrifice

Table 1.

Variables	**Control**	**T2DM**	**T2DM+MSCs**
Fasting glucose (mg/dL)	79.13 ± 5.02	240.6 ± 23.93**a**	155.9 ± 20.02**ab**
Cholesterol (mg/dL)	140.5± 8.89	266.9± 21.02**a**	159.3 ± 3.91**ab**
HDL-C (mg/dL)	65.88± 6.42	26.25 ± 3.84**a**	42.50± 4.17**ab**
LDL-C (mg/dL)	54.13±9.95	215.6±39.44**a**	88.50±7.44**ab**
Body Weight (g)	204.3 ± 5.52	152.0± 5.97**a**	193.1± 10.96**ab**
SBP (mmHg)	92.5 ±4.27	179.8±4.71**a**	121.6±8.33**ab**

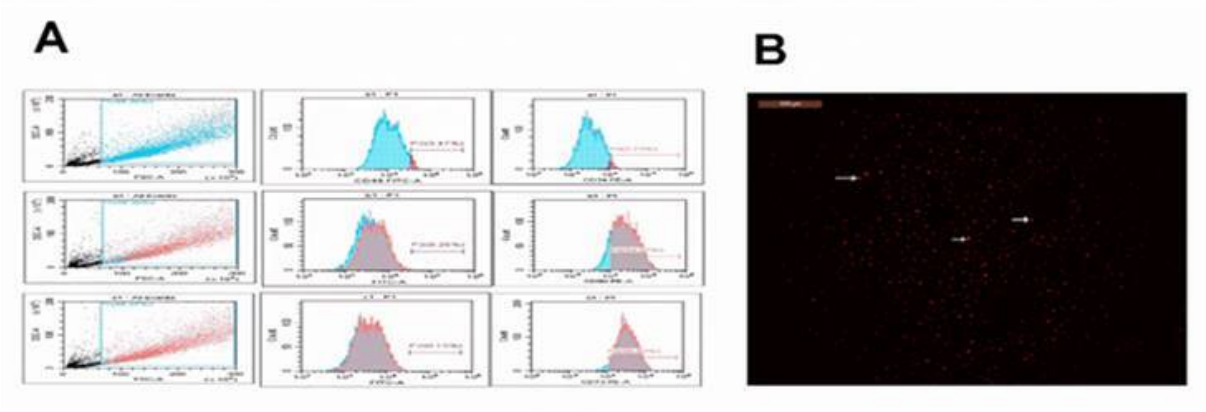

Fig.1(A): BM-MSC identification and characteristics. The immune characteristics of the isolated and cultivated MSCs were used to identify them; they were positive for CD90 and CD73 and negative for CD45 and CD34. BM-MSC characteristics and identification are shown in Fig.1(B). Using a fluorescence microscope to examine cardiac tissue sections, it was possible to see that BM-MSCs labeled with PKH26 fluorescent dye had homing properties (red fluorescence).

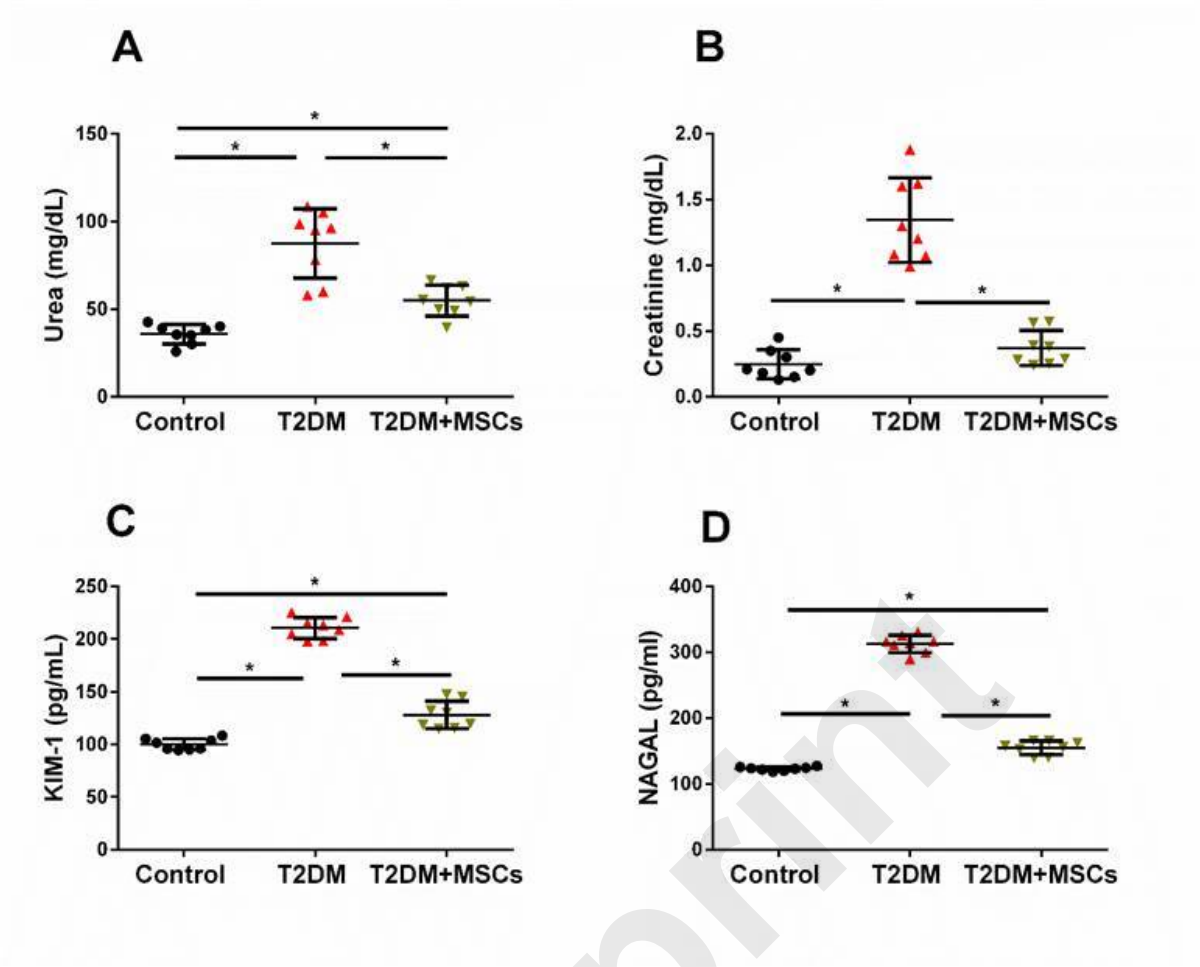

Changes in serum urea (A), creatinine(B), and indicators of kidney injury KIM-1 (C), and NAGAL(D) in control, T2DM, T2DM+MSCs groups. The data is shown as mean ± SD. *: statistically significant in comparison to the control group's corresponding value (P<0.0001) and statistically significant in comparison to the T2DM group's corresponding value (P<0.0001) (n=8).

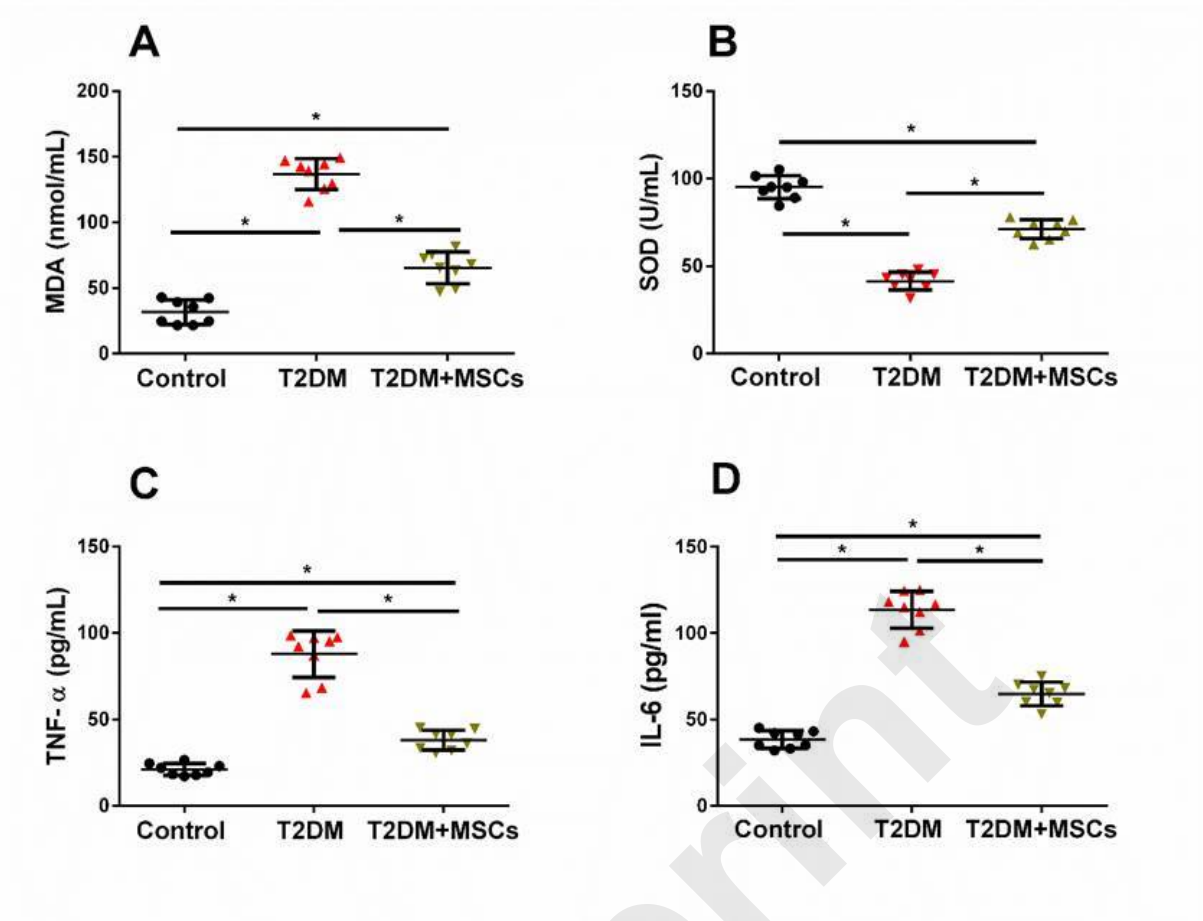

Serum MDA(A) and SOD(B), TNF (C) and IL-6(D) levels changed in the contro, T2DM,, and T2DM+MSC groups. The data are displayed as mean ± standard deviation. *: statistically significant when compared to the comparable value in the control group (P<0.0001) and the T2DM group (P<0.0001) (n=8).

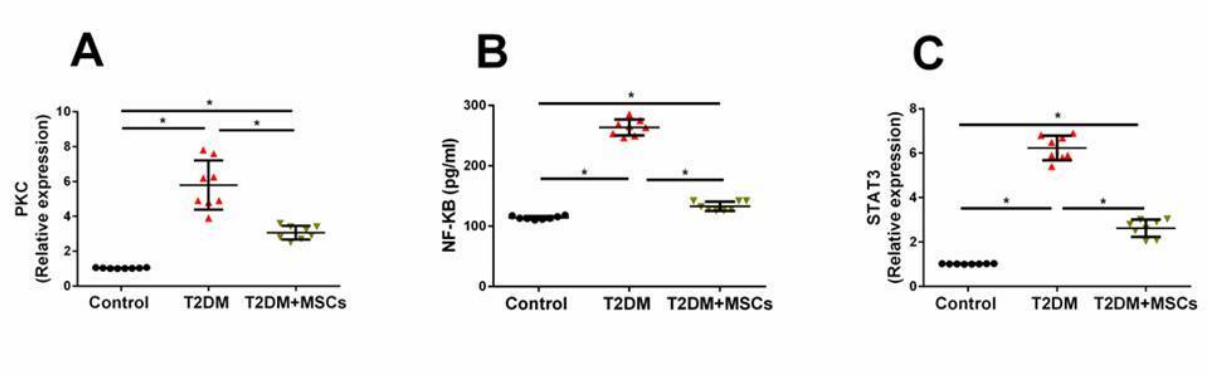

PKC (A), NF-KB (B) and STAT3(C) levels in the control , T2DM, and T2DM+MSCs groups. Information displayed as mean ± standard deviation. *: statistically significant when compared to the equivalent value in the control group (P<0.0001) and the T2DM group (P<0.0001) (n=8).

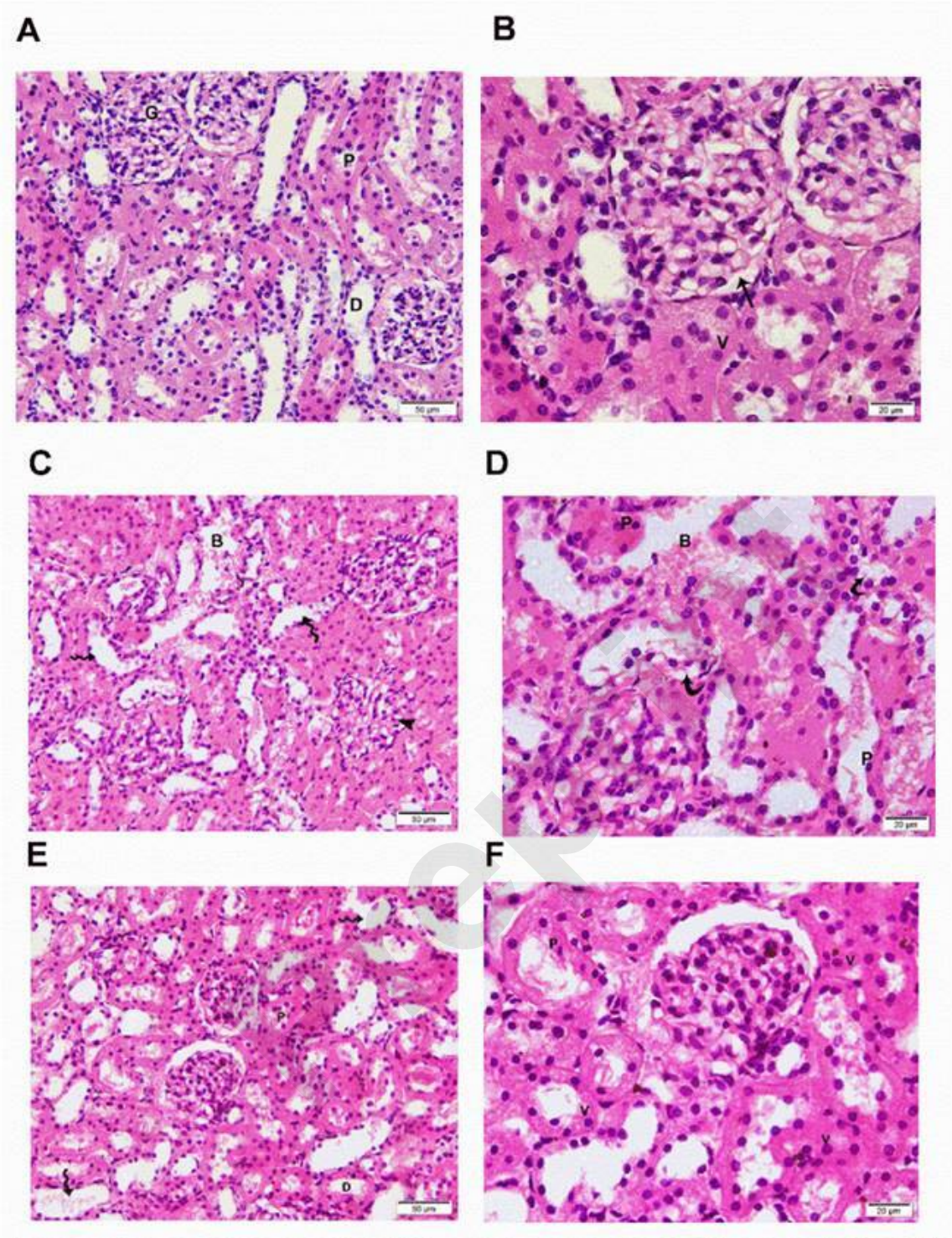

Photomicrographs of H&E-stained sections of the renal cortex. (A, B) Proximal (P) and distal (D) convoluted tubules bordered with cuboidal cells displaying vesicular nuclei (v) and acidophilic cytoplasm; Malpighian renal corpuscle with glomerulus (G); and narrow Bowman's space (arrow) comprise the control group. (A, D) Diabetic group: dilated convoluted tubules (wavy arrow), dilated blood vessels (B), and deformed renal corpuscles (arrowhead). Vacuolated cytoplasm (curved arrow) and tiny, darkly-stained nuclei (P) are visible in the tubular epithelial cells. (F, E) The group known as diabetic+MSCs consists of proximal (P) and distal (D) convoluted tubules bordered with cuboidal cells that display vesicular (v) and acidophilic cytoplasm, but some cells also have pyknotic nuclei (P). There are a few dilated convoluted tubules visible (wavy arrow). (a, d, f ×400; c, e, ×200) (50 μm

and 20 μm scale bars).

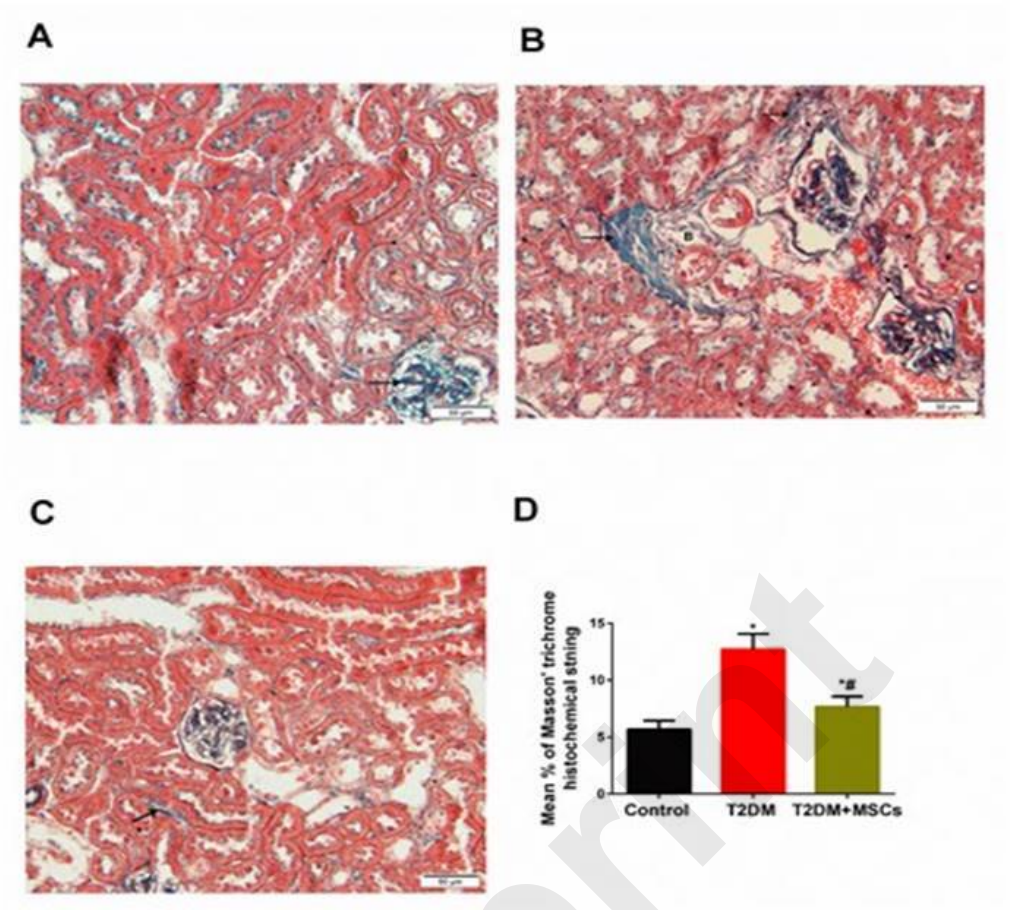

Photomicrographs of Masson-stained sections of the renal cortex. (A) Collagen deposition (arrow) in the glomerulus' interstisium represents the control group. (B) Diabetic group: coarse collagen deposition (arrow) in the deformed glomeruli and renal interstisium between tubules and blood vessels (B). (C) Diabetic+MSCs group: modest localized collagen deposition in the glomeruli and convoluted tubules. (×200) (50 μm scale bar) (D) Calculating the average area percentage of the collagen deposit.

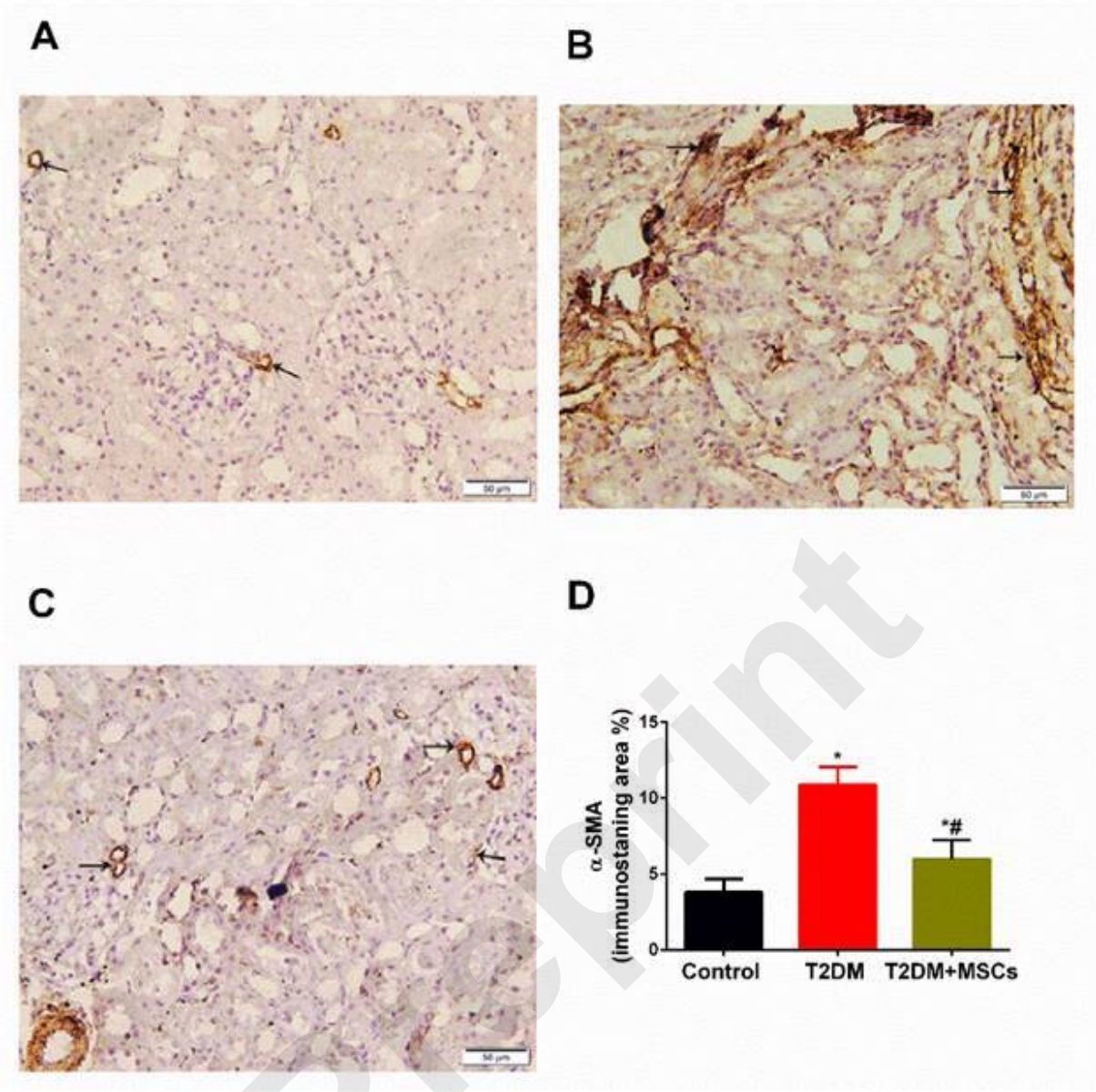

Photomicrographs of α-SMA-stained sections in the renal cortex. (A) Control group : blood vessel walls with modest positive α-SMA immunostaining (arrow). (B) Diabetic group: renal interstisium and blood vessel walls show coarse, widespread positive α-SMA immunostaining (arrow). Minimal positive α-SMA immunostaining (arrow) in the renal interstisium and blood vessel walls (C) Diabetic+MSCs group. (×200) (50 μm scale bar). (D) Calculating the average percentage of α-SMA immunostaining area.

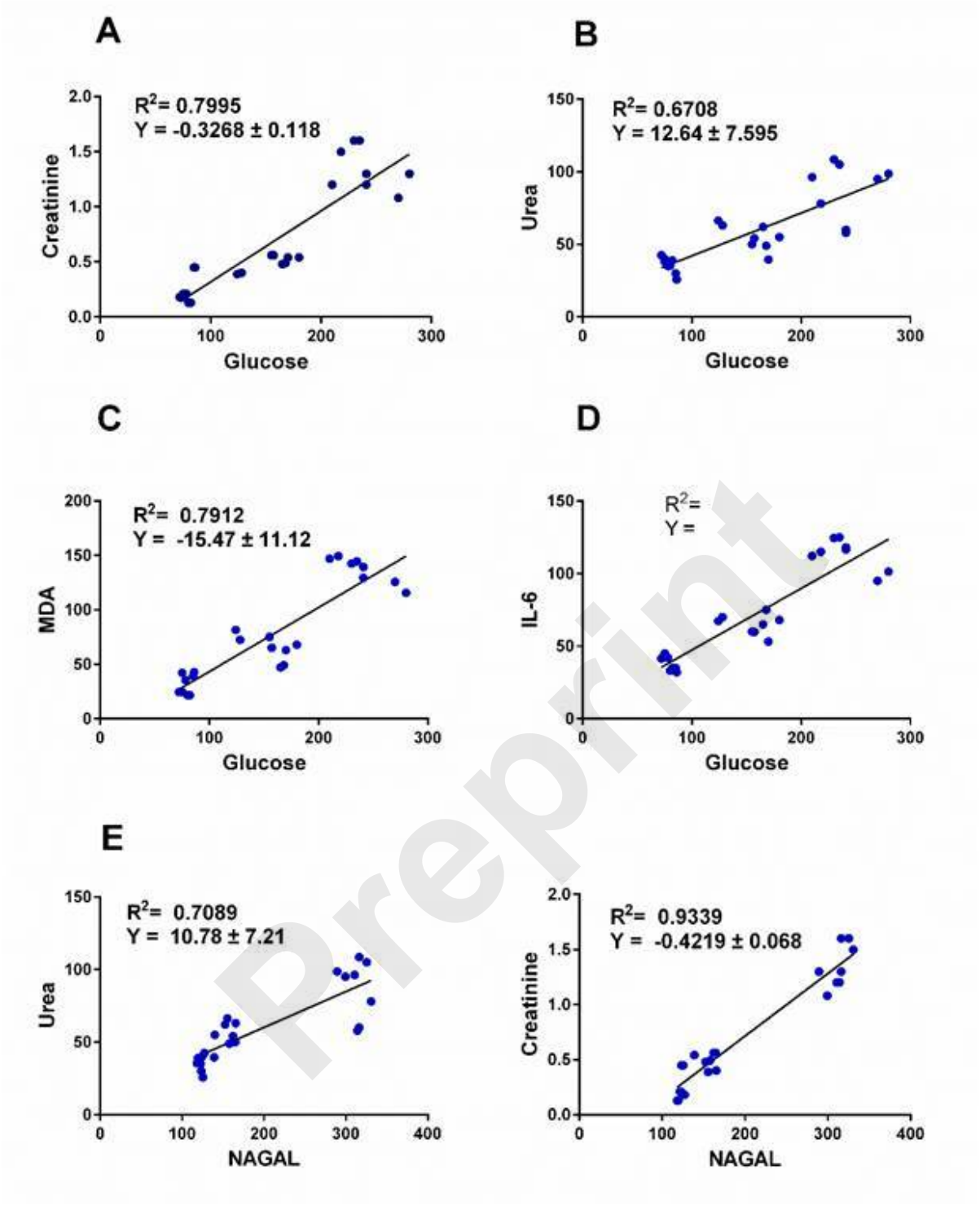

positive correlation between glycemia versus creatinine, urea, MDA, IL-6 (Fig 8A-D). It also showed a positive correlation between NAGAL versus urea and creatinine (Fig 8E-F) ($P < 0.0001$, n=24 for all).

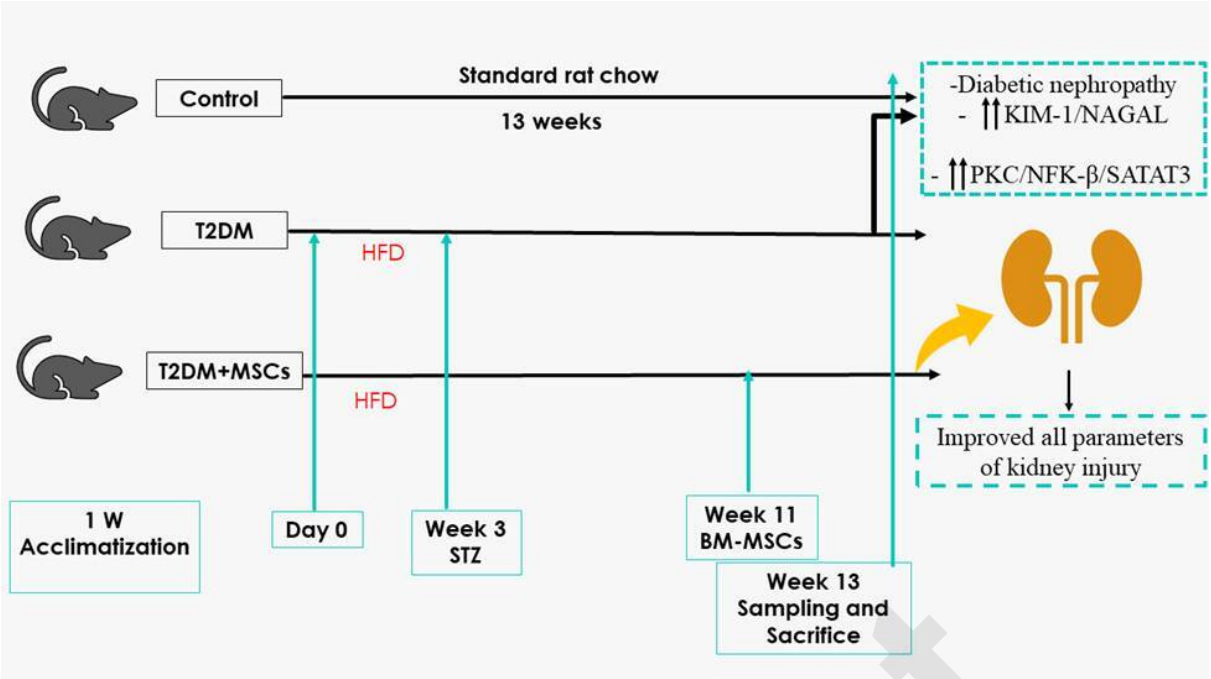

Graphical abstract. Shows that inaction of MSCs ameliorated and improved paremetrs of diabetic nephropathy